Vietnam Journal of Catalysis and Adsorption
Tạp chí xúc tác và hấp phụ Việt Nam

https://jca.edu.vn

Investigation of perovskite catalysts $BaTiO_3$ and $SrTiO_3$ for the oxidative coupling of methane

Phuong Pham Thi Mai[1], Hung Nguyen Thanh[2], Thang Le Minh[2,*]

[1] *International Training Institute for Materials Science, Hanoi University of Science and Technology, Viet Nam*
[2]*School of Chemistry and Life Sciences, Hanoi University of Science and Technology, Viet Nam*
**Email: thang.leminh@hust.edu.vn*

ARTICLE INFO

Received: 20/10/2023
Accepted: 15/12/2023
Published: 30/3/20024

Keywords:
$SrTiO_3$, $BaTiO_3$, OCM, sol-gel

ABSTRACT

In this study, perovskite $BaTiO_3$ and $SrTiO_3$ catalysts were prepared using the sol-gel method for oxidative coupling of methane (OCM). Characterization of catalysts was investigated by X-ray diffraction for crystal properties, physical N_2 adsorption to determine specific surface area, and temperature-programmed techniques to examine the redox properties and acid–base strength. The results showed that at any reaction temperature, the methane conversion of $BaTiO_3$ was consistently higher than that of $SrTiO_3$. This may caused by $BaTiO_3$'s better reducibility detected by H_2-TPR experiments. Moreover, the selectivity of $BaTiO_3$ (25 – 30%) was much greater than that of $SrTiO_3$. Perhaps the abundant lattice oxygen may explain the excellent C_2H_4 selectivity obtained for $BaTiO_3$.

1. Introduction

Methane is a simple gas used extensively to prepare syngas as an indirect path to produce many important chemical blocks [1 - 3]. In order to seek a more sustainable way of utilizing methane, direct conversion of methane to valuable compounds, particularly oxidative coupling of methane for production, such as ethane, ethylene, etc. has attracted much attention from both scientists and manufacturers worldwide. Because of methane's highly stable C – H bond, the OCM reaction must undergo severe conditions such as elevated temperature or high pressure to extract H from methane to prepare methyl radicals, which coupled to form ethane afterward [4,5].

Perovskite, with an ABO_3 formula, where A can be lanthanum, alkali, or alkaline earth metals, and B denotes transition metals, respectively, have been researched widely for the application in oxidative coupling of methane because of their thermal stability, definite structure, high oxygen mobility … [6]. Both $BaTiO_3$ and $SrTiO_3$ have excellent properties suitable for OCM reactions. Therefore, many reports have been published about their catalytic performance over the years. In 2012, based on the $BaTiO_3$'s excellent activity, M. Gharibi and his co-workers employed $BaTiO_3$ as a model sample to investigate the catalytic mechanism and found that the lattice oxygen vacancies could be formed at low energy and only one active site was responsible for the reaction [7]. Significantly, the combination of $BaTiO_3$ and Mn-$NaWO_4$ had good results as higher activity at 100 ^oC lower than used for Mn-$NaWO_4$, which has been known as the best catalyst for OCM until now [8].

Since the advantage of developing the properties led to enhancing the catalytic performance, doping in $SrTiO_3$ has often been studied recently [9, 10]. The results showed that the oxygen mobility and electron transfer

https://doi.org/10.62239/jca.2024.011

were well-improved; consequently, the methane conversion and C_2 selectivity also increased.

In Seoyeon Lim's work [11], $BaTiO_3$ and $SrTiO_3$ were studied for OCM reaction, and it was reported that $BaTiO_3$ had better performance than $SrTiO_3$ at a temperature range from 600 °C to 725 °C under a gas mixture of $(CH_4)/(O_2)/(N_2)$ = 3/1/1 (mol/mol/mol) with gas-hour space velocity of 10 000 h^{-1}. However, the XPS, CO_2-TPD, and O_2-TPD results did not explain clearly the relationship between perovskites' properties and OCM reaction performances. Thus, this paper was expected to reveal this relationship more evidently.

In this paper, the perovskites $BaTiO_3$ and $SrTiO_3$ were prepared by sol-gel and investigated to determine their structure, redox properties, and acid–base strength, remarkably influencing the catalytic activity. Moreover, the OCM reaction was set up at harsh conditions such as high velocity (50 000 h^{-1}), high reaction temperatures (750 °C – 850 °C), and high gas mixture in which a molar ratio of $(CH_4)/(O_2)/(N_2)$ = 4/1/80 (mol/mol/mol) that has not been reported yet. Likewise, it was strongly desired to discover more properties of $BaTiO_3$ and $SrTiO_3$ at high reaction temperatures and velocities to understand these perovskites completely.

2. Experimental

Materials

Ethylene glycol ($HOCH_2CH_2OH$, 99.8%), Barium nitrate ($Ba(NO_3)_2$, Sigma Aldrich) Strontium nitrate ($Sr(NO_3)_2$, Sigma Aldrich), citric acid ($C_6H_6O_8$, 99.5%), Titanium isopropoxide ($Ti[OCH(CH_3)_2]_4$ 97%, Sigma Aldrich) were used to prepare peroskites catalysts.

Preparation of catalyst

Titanium isopropoxide (9.15 mL) was dissolved in ethylene glycol (26.9 mL) and stirred at 60 °C for 30 minutes to obtain a clear solution. DI water (20 mL) was added to titanium isopropoxide and ethylene glycol solution, then stirred at 80 °C for one hour. The solution was cloudy white. After that, citric acid (25.8 g) was added to the solution at 80 °C to make a clear solution of yellow color during vigorous stirring. Then, $Sr(NO_3)_2$ (5.3 g) was added to the above solution and stirred until a viscous gel formed. Next, the gel was air-dried at 200 °C for 12 hours, and the resulting dry powder was calcined in air at 900 °C for 5 hours at a rate of 3 °C/min. Perovskite $BaTiO_3$ was prepared using the same procedure as described above.

Characterization

X-ray powder diffraction (XRD) investigated the samples' crystalline phase. Using Bruker Axs D8 Advance XRD-diffractometer (Germany) with Cu K_α irradiation (40kV, 40 mA), XRD patterns were obtained. The Brunauer-Emmett-Teller (BET) method obtained the specific surface area using a Micromeritics (Gemini VII analyzer). In order to determine the reducing capacity of the oxide surface and the inhomogeneity of the reducing surface, the H_2-TPR measurement is used. Temperature-programmed oxygen desorption (O_2 - TPD) is analyzed to quantify the amount and strength of adsorbed oxygen species. NH_3 determined the acid-base properties – TPD and CO_2 – TPD experiments. The TPx method was analyzed using the Micromeritics Auto Chem II 2920 instrument at Hanoi University of Science and Technology. SEM images were captured on JEOL Benelux equipment in the GeViCat Center, Hanoi University of Science and Technology.

Measurement of catalytic activity

The catalytic performances were determined using a continuous flow reaction system under ambient pressure. For this purpose, catalyst powder (200mg) was granulated with 250 ÷ 450 µm under compressor pressure and placed between a quartz reactor (370 mm height, 5 mm ID). The components as methane (CH_4), oxygen (O_2), and nitrogen (N_2) were introduced to the reactor after passing through a mixer, and the total flow of this gas mixture was fixed at 105mL/min, corresponding to a gas-hourly space velocity (GHSV) of 50,000 h^{-1} determined at 25 °C and 1.5 bar pressure. Catalysts were performed under a gas mixture of CH_4, O_2, N_2, in which molar ratio of $(CH_4)/(O_2)/(N_2)$ = 4/1/80 (mol/mol/mol). The reactions were at 750 °C, 800 °C, and 850 °C, and the products were analyzed by Gas Chromatography (GC) online coupled with Thermo Conductivity Detector and Flame Ionized Detector on the TRACE GC ULTRA system.

The conversion of CH_4 was defined as:

$$\text{Conv (\%)} = \frac{A_{CH_4} - A^*_{CH_4}}{A_{CH_4}} \times 100\%$$

https://doi.org/10.62239/jca.2024.011

Where: Conv (%): Conversion of CH_4

A_{CH4} : Area of bypass peak of CH_4

A^*_{CH4} : Area of the remaining peak of CH_4 after the reaction

Concentrations of C_2H_4 were defined as:

$$C_{C2Hx}\ (\%) = \frac{A_{C_2H_x} \cdot C^*_{C_2Hx}}{A^*_{C_2H_x}}$$

Where: C^*_{C2Hx} was the concentration, and A^*_{C2Hx} was the corresponding peak area of the standard gas flow C_2H_x

Concentrations of CO_2: Determined through a standard curve (Figure 1) between the concentration and the area of the corresponding GC peak. Based on the standard curve, the CO_2 concentration was calculated by the equation below:

$y = 2.72652 * 10 -7 * x + 0.00599$ ($R^2 = 0.998$)

Where:

y: CO_2 concentration (%)

x: Area of CO_2 peak

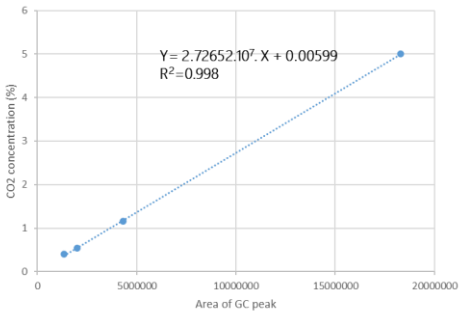

Fig 1: Standard curve $\%V_{CO_2}$

C_2H_x selectivity (%) was defined as:

$$C_{C2Hx}\ (\%) = \frac{C_{C_2H_x}}{C_{C_2H_4} + C_{CO_x} + C_{C_2H_6}} \times 100\%$$

3. Results and discussion

Characterization of catalysts

The X-ray diffraction patterns of the catalysts synthesized by the sol-gel are shown in Figure 2. The results showed that in the $SrTiO_3$ sample, the diffraction peaks at 2θ angle are 22.76°, 32.38°, 39.94°, 46.46°, 52.4°, 57.74°, 67.78°, 72.5°, 77.12° corresponded to the crystal planes (100), (110), (111), (200), (210), (210), (211), (220), (300), (310). The observed peak positions and diffraction pattern matched with the JCPDS (Card No: 01-084-0443) data of the $SrTiO_3$ compound having space group Pm-3m, which indicated the single-phased cubic perovskite structure of the prepared compound [13]. Besides, the characteristic peaks of $BaTiO_3$ at 2θ angle as 22.2°, 32.17°, 38.89°, 45.59°, 50.81°, 56.12°, 65.77°, 70.32°, 74.78°, 79.01° were assigned for the crystal planes (100), (110, (111), (200), (210), (211), (220), (300), (310), (311) [12]. There were no impurities phase on XRD patterns, proving the successful preparation of perovskite catalysts

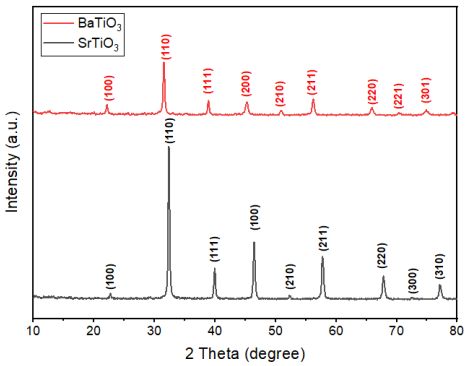

Fig 2: XRD pattern of catalysts

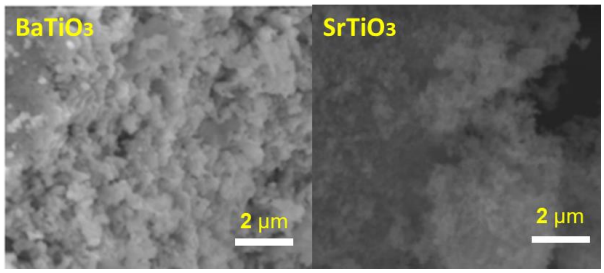

Fig 3: SEM images of catalysts

The specific area of catalysts was determined, and the results showed that the $SrTiO_3$ sample has a higher surface area than $BaTiO_3$, 16 m^2/g and 8.98 m^2/g, respectively. SEM captured the surface of catalysts, and their images in Figure 3 displayed the rough surface with large clusters on both $SrTiO_3$ and $BaTiO_3$. These results were in agreement with the small specific area obtained by BET.

Hydrogen temperature-programmed reduction (H_2-TPR) was performed in the H_2 flow over 100 mg of the material to analyze the reducibility of catalysts. The signal corresponding to H_2 consumption was plotted against temperature and shown in Figure 4 a). Profile of sample $SrTiO_3$ without reduction peak was recorded at temperatures below 400 °C, the broad peak was seen at 575 °C, while the $BaTiO_3$'s profile had two separated desorption peaks at 444 °C and 639 °C. The reducibility of $SrTiO_3$ was the same as the results observed in the

https://doi.org/10.62239/jca.2024.011

investigation of Lei Bai et al. [13]; in addition, the only possible reduction in this system was the reduction of titanium (Ti^{4+} → Ti^{3+}) with simultaneous removal of oxygen from the perovskite structure [14]. As can be seen in Table 1, the amount of H_2 consumption on the $SrTiO_3$ (0.059 mmol/g) was approximate as the value of $BaTiO_3$ desorbed at 444 °C, 0.06 mmol/g; it seems like this desorption peak at 444 °C was also due to the reduction of Ti.

Table 1: Quantification of H_2 consumption by peak integration of H_2-TPR profiles of catalysts

Sample	Temperature (°C)	Quantity (mmol/g)
$BaTiO_3$	444	0.059
	639	0.132
$SrTiO_3$	575	0.066

On the other hand, the $BaTiO_3$ had another desorption peak at 639 °C, which was noticed to reduce bulk lattice oxygen [10]. Thus, it can be noticed that $BaTiO_3$ had better reducibility than $SrTiO_3$ because of the lower reduction temperature of Ti and another reduction of bulk lattice oxygen that $SrTiO_3$ did not have.

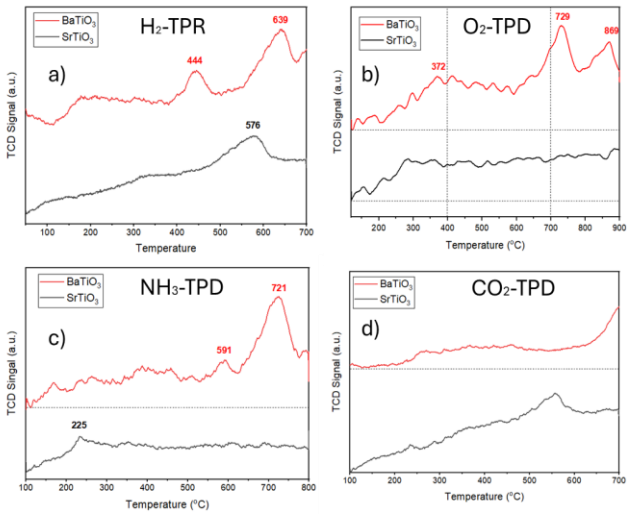

Fig 4: a) H_2-TPR profiles of the catalysts; b) O_2-TPD profiles of the catalysts; c)H_2-TPD profiles of the catalysts; d) CO_2-TPD profiles of the catalyst

The temperature-programmed desorption of O_2 (O_2-TPD) was performed to probe the oxygen species of the catalysts. The results in Figure 4 b) represent no peak recorded for $SrTiO_3$, while three peaks at 372 °C, 729 °C, and 869 °C are observed in the case of $BaTiO_3$. Generally, the desorption peak below 550 °C accounted for adsorbed oxygen species that desorbed from surface or lattice oxygen coming from dislocations; thus, the desorption peak at 372 °C on $BaTiO_3$ perhaps assigned for the availability of oxygen from vacancies on the surface or very near the surface. Nevertheless, the desorption peak at higher 700 °C would be the oxygen released from the inner layers of the lattice, which can cause a reduction of Ti as a B site cation in this $BaTiO_3$ perovskite [15].

The acid–based properties of catalysts were examined by TPx, and the results are shown in Figure 4 c) and d). The NH_3 desorption peak was detected at 225 °C on $SrTiO_3$, which inferred that some weak acidic sites present on the catalyst surface. On the other hand, in the case of $BaTiO_3$, there were two NH_3 desorption peaks at 591 °C and 721 °C, accounting for mid-strong and strong acid sites [16]. The basicity of catalysts was evaluated by CO_2-TPD measurement, and the profiles are displayed in Figure 4 d). It is noticed that the desorption peaked at 550°C on the $SrTiO_3$ profile, meaning the presence of a mid-strong primary site, while another significant CO_2 evolution was observed at 700°C on the $BaTiO_3$ profile, which accounted for a strong basic site.

Catalytic activity

The catalysts were employed for the OCM reaction in the temperature range from 750 to 850 °C, and the performances are shown in Figures 5 a) and b). In Figure 5 a), as the reaction temperature increased, the CH_4's conversion of $SrTiO_3$ went from 8% to 15%. Additionally, the $BaTiO_3$ rose from 14.5% to 16%. As can be seen in the H_2-TPR results, the better reducibility of $BaTiO_3$ was also explained for higher methane conversion than that of $SrTiO_3$. Moreover, it was fascinating to obtain the C_2H_4's selectivity of $BaTiO_3$ ranged from 25 to 30 %, while the $SrTiO_3$ was about 0.8% at 800 °C in Figure 5 b).

During the OCM reaction, alkaline sites converted the methane to the methyl radical. Therefore, mid-strong and strong basic sites were considered as the essentially active sites for selectively activating methane to C_2 hydrocarbon. According to CO_2-TPD results, $SrTiO_3$ and $BaTiO_3$ had these critical sites but with different strengths. As a result, these catalysts could convert methane at reaction temperatures from 750 to 850°C. Nonetheless, the alkaline sites originate from oxygen anions (O_2^-, O_2^{2-}, O^{2-}) on the catalysts' surface. These surface oxygen species were consumed and transformed into vacancies, which can be refilled from

https://doi.org/10.62239/jca.2024.011

the gas phase or lattice oxygen [10]. As in H_2-TPR results, not only $SrTiO_3$ but also $BaTiO_3$ had available lattice oxygen, which could quickly fill vacancies and continue to produce the alkaline sites in the OCM reaction. Besides, the lattice oxygen species had another important role in determining the selectivity of the OCM reaction. It is said that the lattice oxygen species with different binding energies led to dissimilar products of the OCM reaction. In primary, the lattice oxygen species with high binding energy and weak binding to metal promoted the conversion of CH_4 to CO, subsequently to CO_2 with adsorped surface O species. In addition, the lattice O species with moderate binding to metal and binding energy were responsible for producing C_2 products. According to the O_2- TPD profile of $BaTiO_3$, it can be noted that the lattice oxygen species at 729 and 869 °C were perhaps in the group that was suited to form C_2H_4 selectively. Indeed, the selectivity of C_2H_4's $BaTiO_3$ ranged from 25 to 30 % during the OCM reaction.

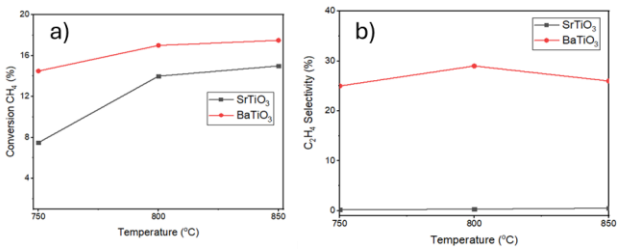

Fig 5: a) Catalytic activities of catalysts for the OCM reactions in the presence of oxygen; b) C_2H_4 selectivity of catalysts

On the other hand, the lattice oxygen species strongly bonded to metal, resulting in low catalytic activity because of its high stability; it seems like $SrTiO_3$ was this case. In fact, the C_2 selectivity of this catalyst was only 0.8% at any temperature reaction. Though there are not any O_2 evolution peak on the $SrTiO_3$ profile, the presence of lattice O species is still noted by the H_2 desorption peak at 575 °C, and this O species strongly bind to metal, leading to low selectivity. In conclusion, both methane conversion and C_2H_4 selectivity of $SrTiO_3$ were worse than that of $BaTiO_3$ because $BaTiO_3$ had better reducibility and significant lattice oxygen species than the remaining one.

4. Conclusion

Perovskite $BaTiO_3$ and $SrTiO_3$ catalysts were prepared and fully characterized to investigate their properties and explain their catalytic activities in OCM reactions. The formation of delicate crystalline phases was shown on the XRD patterns. These two perovskites had a cubic phase. The BET method determined and captured the perovskite surface using the SEM method. The specific area of $BaTiO_3$ was slightly higher than that of $SrTiO_3$, at 16 m^2/g and 8.98 m^2/g, respectively. In addition, the SEM images of two perovskites were consistent with the low BET area. From H_2-TPR results, the lower temperature of desorption peak at 444 °C was one of the strong points that proved $BaTiO_3$ has better reducibility than $SrTiO_3$. Consequently, $BaTiO_3$ always had higher methane conversion than $SrTiO_3$ at any reaction temperature. Furthermore, the CO_2- TPD results determined the mid-strong and strong basic sites of these perovskites, which confirmed the capacity of both $BaTiO_3$ and $SrTiO_3$ to activate methane.

Regarding selectivity, the O_2-TPD was performed to elucidate the lattice O species, which was the critical factor for C_2 selectivity. In $BaTiO_3$'s profile, there were three evolution peaks at 372 °C, 729 °C, and 869 °C, while no peak in $SrTiO_3$'s profile. It is said that the desorption peak at 372 °C was accounted for adsorped O species, which could quickly refill the oxygen vacancies, resulting in high CH_4 conversion through the oxygen cycle during the reaction. On the other hand, the desorption peaks at 729 °C and 869 °C were assigned for lattice O species having moderate binding energy and moderate binding to metal. Hence, these lattice O species were responsible for $BaTiO_3$'s high C_2H_4 selectivity as 25 % – 30 % when the temperature reaction ranged from 750 °C to 850 °C.

Acknowledgments

This research is funded by Hanoi University of Science and Technology (HUST) under project T2021-SAHEP-017.

References

1. Keller, G. E., M. M. Journal of Catalysis 73.1 (1982) 9-19. https://doi.org/10.1016/0021-9517(82)90075-6
2. Enger, B.C., Lødeng, R. and Holmen, A. Applied Catalysis A: General 346.1-2 (2008) 1-27. https://doi.org/10.1016/j.apcata.2008.05.018
3. Pereñíguez, R., González-DelaCruz, V. M., Holgado, J. P., & Caballero, A. Applied Catalysis B: Environmental 93.3-4 (2010) 346-353. https://doi.org/10.1016/j.apcatb.2009.09.040
4. Beck, B., Fleischer, V., Arndt, S., Hevia, M. G., Urakawa, A., Hugo, P., & Schomäcker, R. Catalysis Today 228 (2014). 212-218. https://doi.org/10.1016/j.cattod.2013.11.059
5. Lomonosov, V. I., and M. Yu Sinev. Kinetics and Catalysis 57.5 (2016) 647-676. https://doi.org/10.1134/S0023158416050128

6. Silvia Carlotto. Applied Surface Science (2022). https://doi.org/10.1016/j.apsusc.2022.154376
7. M.Gharibi, M. S. Motallebipour. Oxidation Communication 35, No 3, 525 – 537 (2012)
8. Lien Thi Do, Jae-Wook Choi, Dong Jin Suh, Chun-Jae Yoo, Hyunjoo Lee, Jeong-Myeong Ha. Applied Catalysis B: Environmental 298 (2021) 120553. https://doi.org/10.1016/j.apcatb.2021.120553
9. Seoyeon Lim, Jae-Wook Choi, Dong Jin Suh, Kwang Ho Song, Hyung Chul Ham, Jeong-Myeong Ha. Journal of Catalysis 375 (2019) 478-492. https://doi.org/10.1016/j.jcat.2019.04.008
10. Yue Wang, Xiao Yang, Chenxiao Hou, Fumin Yin, Guowei Wang, Xiaolin Zhu, Guiyuan Jiang, Chunyi Li . ChemCatChem 13 (2012) 4182 - 4191. https://doi.org/10.1002/cctc.202100859
11. Lim, S., Choi, J. W., Suh, D. J., Song, K. H., Ham, H. C., & Ha, J. M . Catalysis Today 352 (2020) 127-133. https://doi.org/10.1016/j.cattod.2019.11.014
12. Monika Singh, B.C.Yadav, Ashok Ranjan, Manmeet Kaur, S.K. Gupta. Sensors and actuators b : chemical 241 (2017) 1170 - 1178. https://10.1016/j.snb.2016.10.018
13. Lei Bai, Felipe Polo-Garzon, Zhenghong Bao, Tian, Zili Wu. ChemCatChem 11 (2019) 2107 – 2117. https://doi.org/10.1002/cctc.201900159
14. Kang Wu, Yuhai Sun, Liu Jing, Xiong Juxia, Junliang Wu, Jin Zang, Fu Mingli, Chen Limin, Haomin Huang, Daiqi Ye. Journal of Hazadous Materials 405 (2021) 124156. https://doi.org/10.1016/j.jhazmat.2020.124156
15. Jon A. Onrubia, B. Pereda-Ayo, U.De-La-Torre, Joan R. González-Velasco. Applied Catalysis B: Environmental 213 (2017) 198–210. https://dx.doi.org/10.1016/j.apcatb.2017.04.068
16. Glorius Maja, Monica AC Markovits, Cornelia Breitkopf. Catalysis 8.9 (2018) 358. https://doi.org/10..3390/catal8090358